International Journal of Heat and Fluid Flow 29 (2008) 957–966

Contents lists available at ScienceDirect

International Journal of Heat and Fluid Flow

journal homepage: www.elsevier.com/locate/ijhff

Influence of a synthetic jet excitation on the development of a turbulent mixing layer

J.-P. Bonnet*, W.L. Siauw, S. Bourgois [1], J. Tensi

Laboratoire d'Etudes Aérodynamiques, Université de Poitiers – ENSMA, CNRS, Téléport2, 1, Avenue Clément Ader, BP 40109, 86961 Futuroscope Chasseneuil Cedex, France

ARTICLE INFO

Article history:
Received 2 November 2007
Received in revised form 28 March 2008
Accepted 2 April 2008
Available online 4 June 2008

Keywords:
Mixing layer
Flow control
Synthetic control jets
Turbulence

ABSTRACT

This paper concerns the experimental study of the control of a turbulent plane mixing layer by a single array of synthetic (loudspeakers) jets deployed through circular orifices. The displacement of the mixing layer towards the wall partially mimics the flow control scenario of the reattachment of a massively separated flow with the jets positioned after the separation location. The experimental setup is the mixing layer downstream of a splitter plate positioned at a small distance away from a flat plate. PIV observations show that the synthetic jet abruptly destroys the large scale coherent structures. There is a large modification to the turbulence field due to the distortion in the mean velocity field. An overall increase in the mixing of the flow between the flat plate and the mixing layer which cause the deviation of the flow towards the wall surface. Lastly, a parametric study of the synthetic jet trajectory is realized by varying the velocity of the air stream that generates the mixing layer. The ratio of the peak jet velocity to the lower velocity of the mixing layer should not be overly excessive such that the jet penetrates the mixing layer completely.

1. Introduction

In most flow separation control strategies, the actuators are placed upstream of the location of the separation so that the actuators perturb the boundary layer structure. This induces extra vorticity which enhances the momentum transfer towards the wall, and the energized boundary layer is more resistant towards adverse pressure gradients. A different strategy had been adopted by Viswanath et al. (2000); they placed a tangentially orientated jet within a separation bubble and demonstrate its efficiency. In this case, the physics of the interaction between the control jets and the separated layer is different from deploying a jet upstream of the separation location. Such control can be a unique tool for controlling massively separated flow without completely attaching it. The study of Bourgois (2007), which motivated the current study, showed that a separated boundary layer over a NACA0015 airfoil could be reattached by introducing a synthetic jet excitation within the separated region. This has potential application in the case when separation occurs due to geometrical effects encountered in the aft of bluff bodies such as rear panels of cars.

In order to characterize this control method, we define a simple and fundamental flow configuration composing of a turbulent mixing layer developing in non-symmetric external conditions, such that one wall of the wind tunnel is closer than the other from the mixing layer axis. This configuration represents a mixing layer developing close to the wall. It has some similarity to a separated flow over a solid surface, some distance downstream from the separation location. Due to the effects of entrainment, the dissymmetry of the external field will impose more modification on the side of mixing layer (low velocity side) that is closer to the wall as compared to the other side that can be considered to be interfaced with an infinite environment. It is then expected that, any action on the mixing process of the mixing layer will be enhanced by the dissymmetry in external conditions. In the present situation, a shear layer originates from the end of the splitter plate separating two air streams of different speed. For the case of flow separation over an airfoil, the origin of the shear layer arises from a separation from a wall surface. Its physics is complicated by the effects of adverse pressure gradient and the presence of re-circulation. In essence, the present configuration is designed to control a mixing layer close to a wall surface that simulates a shear layer arising from a separation which could be topologically close or open. Practically, it would bear some resemblance to the flow at the trailing edge of a main element-flap junction of a high lift system. A single array of synthetic jets perturbing a turbulent mixing layer is used as a simplified model for the study of deploying the jets within a separated zone. The actuator system, developed in the work of Bourgois

* Corresponding author. Tel.: +33 549366031; fax: +33 549366001.
E-mail address: jean-paul.bonnet@univ-poitiers.fr (J.-P. Bonnet).
[1] Present address: Snecma Groupe SAFRAN - Site de Villaroche, Département Chambres et Systèmes Futurs, Rond Point René Ravaud, 77550 Moissy Cramayel, France.

0142-727X/$ - see front matter © 2008 Elsevier Inc. All rights reserved.
doi:10.1016/j.ijheatfluidflow.2008.04.004

(2007), is installed in a flat plate and positioned below a developed turbulent mixing layer. The aim of this experimental approach is to have a better insight to the understanding of the mechanisms which drive the boundary layer reattachment.

2. Experimental facility and flow arrangement

The flat plate model is mounted into the test section ($1.25 \times 1.25\ m^2$) of an open loop wind tunnel. The chord of the plate is 1 m and has a span measuring 1.25 m. A splitter plate is used to generate the mixing layer as described in Fig. 1. The distance from the upper wall of the wind tunnel is 400 mm and the lower wall is 55 mm (~1.8 times the vorticity thickness of the mixing layer) away from the axis of the mixing layer. This will provide an approximate representation of the situation of a shear layer in a separated flow over a solid surface. Fig. 1a shows the experimental arrangement. The origin ($x = 0$ mm) of the streamwise coordinate is located at the actuator location because it is the source of the perturbation in the flow. Significant changes to the flow are expected downstream from this position. The vertical origin ($y = 0$mm) is specified as the trailing edge of the splitter plate. The trailing edge is located upstream of the actuator location such that the mixing layer is developed and reaches a quasi-asymptotic state. The coordinates of the trailing edge of the splitter plate are $x = -286$ mm and $y = 0$ mm. A flat plate, with a bevel of 15° simulating the rear part of an airfoil, is installed below the splitter plate such that $x = 184$ mm and $x = 424$ mm mark the beginning of the bevel and the end of the flat plate, respectively. The parameters used to characterize the mixing layer are the velocity ratio (r), the mean velocity (U_m), the velocity difference (ΔU) and the velocity parameter (λ) which are defined as follows: $r = U_2/U_1$, $U_m = (U_1 + U_2)/2$, $\Delta U = U_1 - U_2$, $\lambda = \Delta U/2U_m$.

Synthetic jets through circular orifices are generated by loudspeakers installed within the flat plate; five jets are controlled by one loud speaker. The frequency of the jets can be adjusted between 20 and 100 Hz. The jet axis is orientated normal to the wall. The diameter of the circular orifices (d_j) is 3 mm and the spacing between two jets in the spanwise direction is 10 mm. A similar jet deployment technique was used by Darabi and Wygnanski (2004). They used loud speakers to generate a synthetic jet through a slot to control separation over a generic flap. In the case of Amitay and Glezer(2002), they used synthetic jets deployed through a rectangular slit near the modified leading edge of a four digit symmetric NACA series airfoil and successfully suppressed flow separation up to post stall angles of attack. In the present study, a frequency of 100 Hz is selected based on the large extent of mixing layer deviation observed via laser light sheet visualization. Ho and Huerre (1984) pointed out that better efficiency could be expected if an appropriate frequency has been chosen to perturb the mixing layer instability. Another concept concerning the use of a frequency scaled by the size of the separation and free stream velocity such that it is equal to unity has been used by Darabi and Wygnanski (2004). Hong et al. (2002) demonstrated a different mechanism; they perturbed the boundary layer instability (Tollmien–Schlichting instability) to achieve efficient control of the laminar separation bubble using synthetic jets deployed via loud speakers. Fig. 2a shows the variation of the velocity output at the exit plane of the orifice when operating at a 100 Hz. This measurement was made with a single component hotwire with a length of 1.5 mm and would give an approximate of the space average 'rectified' velocity. A sampling frequency of 10 kHz was used. The synthetic jet encounters the mixing layer at a vertical position typically 30 mm (~10 diameters) away from the orifice. At that location, the suction phase of the synthetic jet is not present which is consistent with previous experimental results reported in Bourgois (2007).

The spanwise characteristic, in terms of velocity fluctuation, of the jet in the presence of a cross flow is presented in Fig. 2b. At $x = 10$ mm, large fluctuation localized at adjacent sides of the orifices are induced by the jet creating a wavelike distribution throughout the span. This fluctuation gets smeared out and displaced from the wall surface in the downstream location at $x = 25$ mm.

3. Results

3.1. Deflection of a mixing layer in near field of the jet

The results presented in this section are obtained by PIV. The pulse between the Nd-Yag laser was set at 250 μs in order to resolve the dynamics of the jet region. The resolution of the camera is 1375 by 1039 pixels, velocity vectors are calculated by sequen-

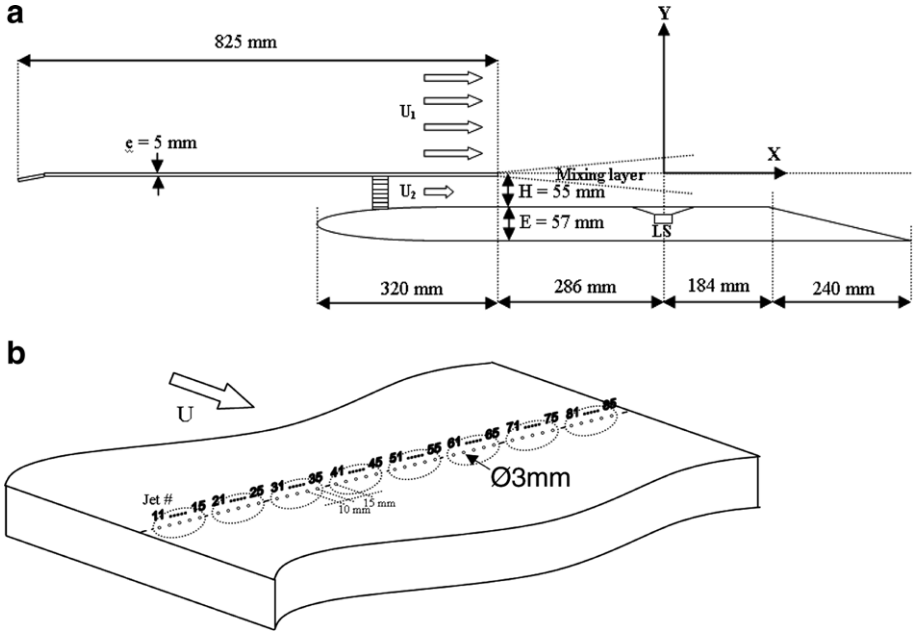

Fig. 1. (a) Experimental arrangement and (b) distribution of orifices at $x = 0$ mm.

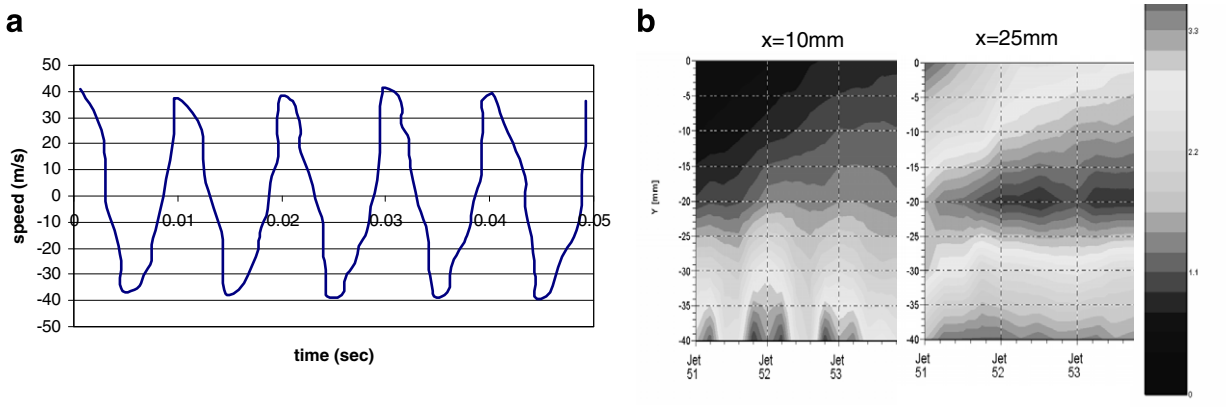

Fig. 2. (a) Variation of velocity at the exit plane of the orifice when deployed at 100 Hz without cross flow and (b) streamwise velocity fluctuation, distributed over three synthetic jets in the spanwise direction, measured by a single component hot wire at $x = 10$ mm and 25 mm in the presence of cross flow with $U_1 = 4.8$ m/s.

tial cross-correlation in an interrogation window of 16 by 16 pixels with a 50% overlap ratio. The PIV observation window was placed directly above an orifice at a position corresponding to 1/3 span of the flat plate. The calculation was performed by the commercial software, LaVision. The uncontrolled (baseline) flow conditions are tabulated in Table 1, where Λ is the ratio of the orifice diameter to the boundary layer thickness.

The mean velocity profiles for uncontrolled and controlled cases are presented in Fig. 3a and b, respectively. The order of magnitudes of the Reynolds stress at $y \sim 0$ mm, in Fig. 4, is consistent with a classical mixing layer. The mean streamwise velocity contours, for the uncontrolled case, is presented in Fig. 5a. It can be observed that the flow is slightly displaced towards the lower wall, as expected due to asymmetric location of the splitter plate. The corresponding distribution of the vertical component velocity, in Fig. 6a, shows a small deflexion effect towards the wall. With reference to (Figs. 5b and 6b, the deployment of the synthetic jets causes a strong distortion in velocity field in the region where $y < 0$ mm and $x > 0$ mm. A comparison of the streamwise velocity profile between the uncontrolled and controlled case suggests that the mean shear is displaced toward the wall (see Fig. 3). In addition, the activation of the synthetic jet results in an acceleration of the flow in the low velocity side of the mixing layer ($0 \text{ mm} < y < -30$ mm). After $x = 0$ mm, as shown in Figs. 7 and 8, very large level of turbulence are observed. These are associated to the high velocity gradients generated at the interface of the control jet and the deviated mixing layer. This can be a characteristic feature of an attaching flow due to the deployment of synthetic jets within the separated region. The increase of the mixing is associated to an increase of the entrainment process. The extra entrainment should correspond to a need for extra debit that has to be extracted from the equivalent channel flow in the part of flow between the mixing layer and the wall. This explains qualitatively the deviation of the mixing layer. In contrast, the synthetic jet does significantly affect the flow in the region where $y > 0$ mm.

Table 1
Characteristics of the baseline mixing layer

U_1 (m/s)	r	U_m	ΔU	Λ
4.8	0.63	3.96	1.69	0.21

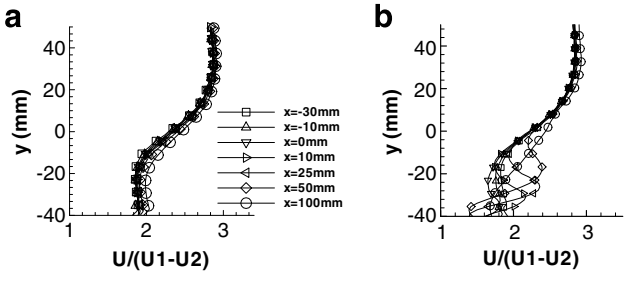

Fig. 3. Mean U velocity profiles at various x positions: (a) uncontrolled and (b) controlled flow, with synthetic jets deployed at 100 Hz.

The turbulence production term,

$$P = \frac{-\left[\langle v'^2\rangle \frac{dV}{dy} + \langle u'^2\rangle \frac{dU}{dx} + \langle u'v'\rangle \left(\frac{dU}{dy} + \frac{dV}{dx}\right)\right]}{(\Delta U)^3}$$

for the baseline flow is shown in Fig. 9a and is overall positive. However, when the control is deployed, as shown in Fig. 9b, there is a localized region near the jet with negative production and is clear that the original mixing layer (for $x > 0$ mm) has been totally modified such that the production in the downstream direction is more distributed towards regions where $y < 0$ mm. The mean velocity profiles, in Fig. 3b, indicates an increase in velocity and momentum in this region. Moreover, inspection of the controlled velocity profile

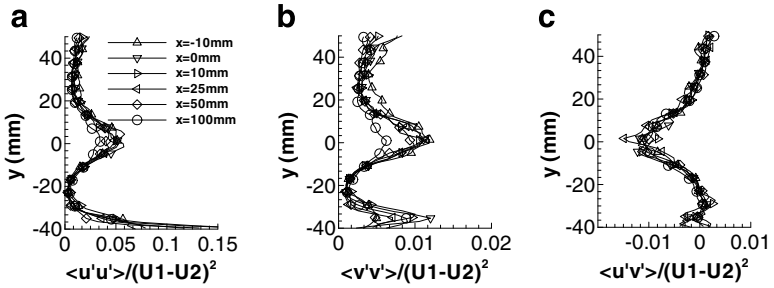

Fig. 4. Reynolds stress profiles at various x positions: (a) $\langle u'u'\rangle/(\Delta U)^2$; (b) $\langle v'v'\rangle/(\Delta U)^2$; and (c) $\langle u'v'\rangle/(\Delta U)^2$ in the uncontrolled flow.

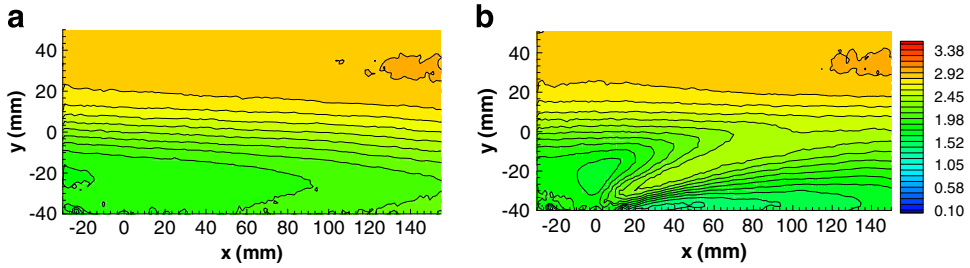

Fig. 5. Mean velocity fields ($U/\Delta U$) for (a) uncontrolled and (b) controlled flow with jets deployed at 100 Hz.

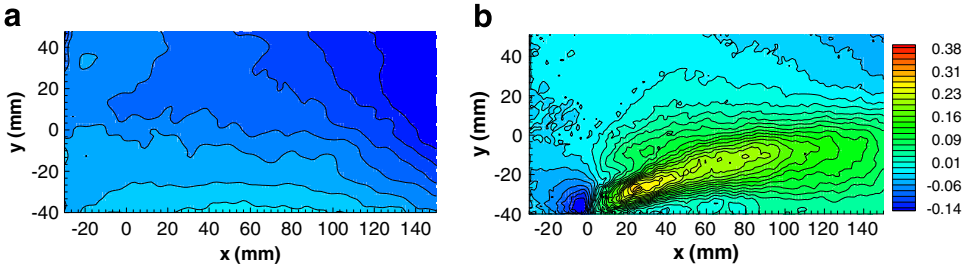

Fig. 6. Mean velocity field ($V/\Delta U$) for (a) uncontrolled and (b) controlled flow with jets deployed at 100 Hz.

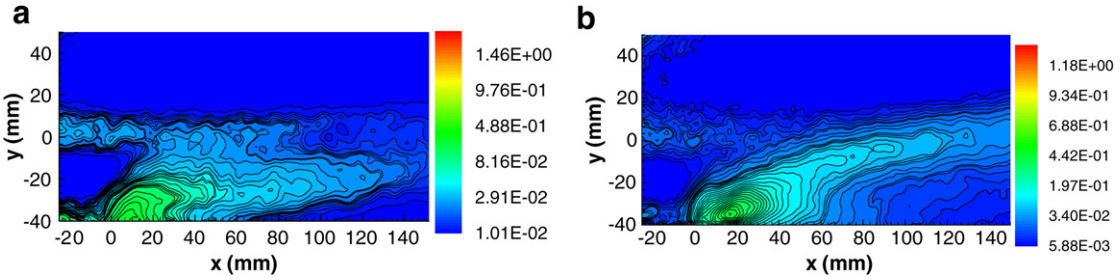

Fig. 7. Controlled flow Reynolds stress fields: (a) $\langle u'u' \rangle/(\Delta U)^2$; and (b) $\langle v'v' \rangle/(\Delta U)^2$, with jets deployed at 100 Hz.

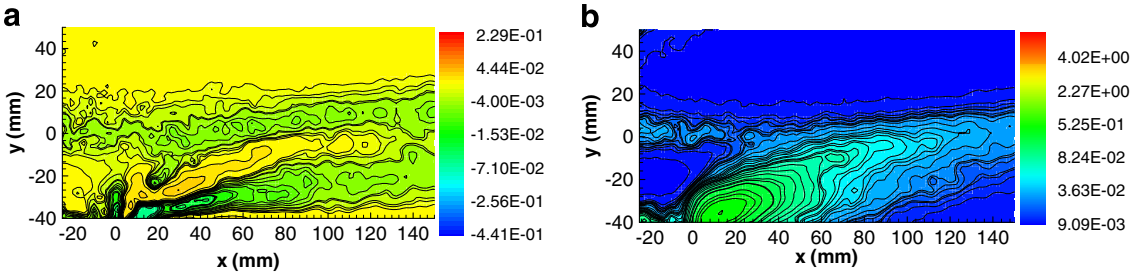

Fig. 8. Controlled flow: (a) Reynolds stress field $\langle u'v' \rangle/(\Delta U)^2$; and (b) turbulent energy, with jets deployed at 100 Hz.

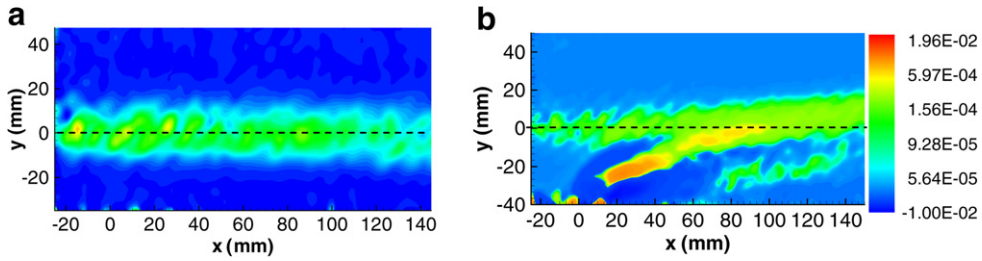

Fig. 9. Turbulence production field: (a) uncontrolled; and (b) controlled flow, with jets deployed at 100 Hz.

at $x = 100$ mm indicates a widening of the vorticity thickness by 13% as compared to the uncontrolled case. These observations explain the shift of the original mixing layer axis towards $y < 0$ mm for the interval 0 mm < x < 140 mm. There is also a slight spread in regions where $y > 0$ mm, but the associated mean velocity profile remains unchanged when we compare Fig. 3a and b. Note that the original mixing layer still remains in the region of $x < 0$ mm. It should be remarked that the flow modified flow field is no longer a mixing layer. However, it bears the characteristics of a mixing layer shifted towards the wall after $x = 100$ mm.

3.2. POD analysis of the interaction of the synthetic jet and the mixing layer

In order to visualize and extract information concerning the large eddies due to synthetic jet and interaction with the uncontrolled mixing layer for the case described in Section 3.1, the technique of Proper Orthogonal Decomposition (POD), originally proposed by Lumley (1967) and applied in a mixing layer by Delville et al. (1999), has been applied to the uncontrolled and controlled cases. Each case comprises of 500 independent realizations. The snapshot POD has been used and the decomposition is defined according to

$$u_i(x,y,t) = u_{\mathrm{mean},i}(x,y) + \sum_{n=1}^{N} a^n(t)\Phi_i^n(x,y), \quad i = 1,2,$$

$$u_1 = U \text{ and } u_2 = V,$$

where N is the total number of modes, $a^n(t)$ are the fourier coefficients, Φ^n are the spatial modes, $u_{\mathrm{mean},i}$ is the temporal mean of 500 realizations of velocity fields and t denotes time. The spatial modes of the uncontrolled flow follow that of a conventional mixing layer as shown in Fig. 10. The region of main activity is centered about $y = 0$ mm. The first two spatial modes of the controlled flow in Fig. 11a and b revealed 2 shear layers due to the synthetic jet. This is probably due to the separated shear layer from the circular orifice. If we view the system of structures in a coordinate system that is orthogonal to an imaginary jet trajectory, we would have a series of counter rotating pairs of vortices. These structures can be interpreted as a series of vortex rings in three dimensions as in the work of Yehoshua and Seifert (2006), when they deployed a

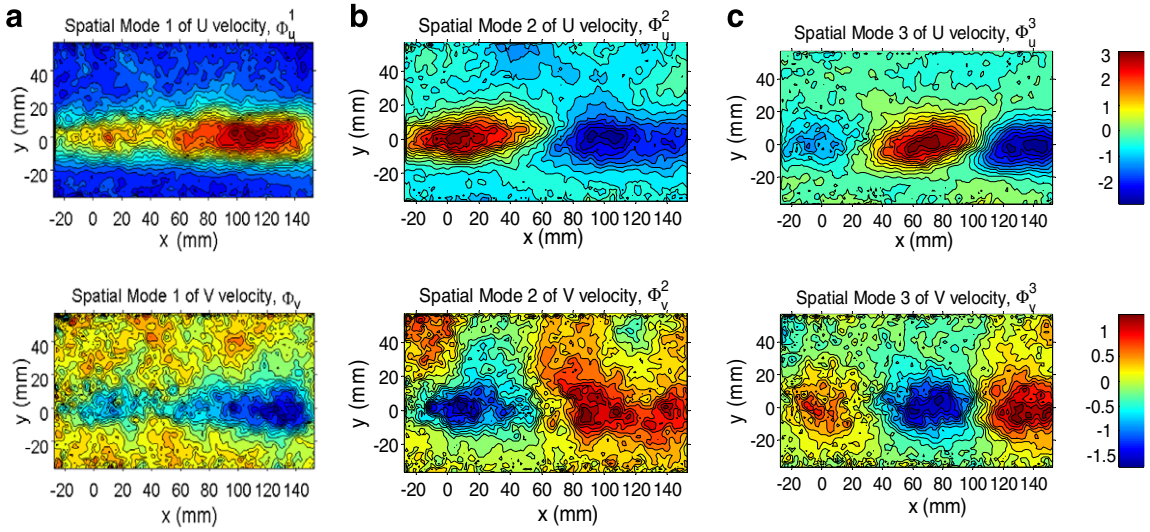

Fig. 10. Spatial modes for U and V velocities for the uncontrolled flow: (a) first; (b) second; and (c) third mode.

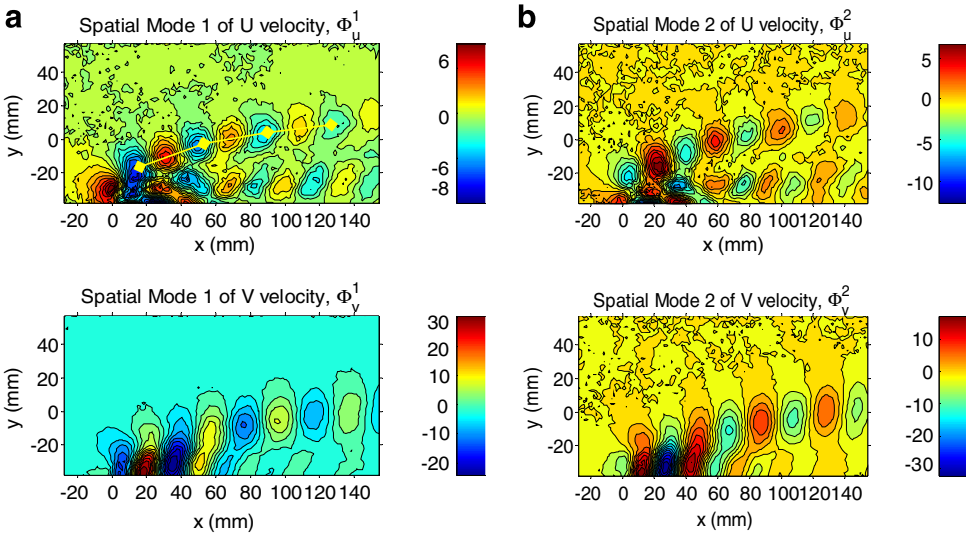

Fig. 11. Spatial modes for U and V velocities for controlled case: (a) first; and (b) second mode.

normal synthetic jet in the presence of a cross flow. As shown in Fig. 11a, the length scale between vortex rings is approximately 40 mm. Spectral analysis of the velocity (not presented) revealed a dominant 100 Hz in the region of the coherent structure, a convective speed of these structures can be estimated as 4 m/s (=40 mm × 100 Hz).

The typical frequency of the velocity in the uncontrolled mixing layer is ~30 Hz (approximately one third of the activation frequency) at the location of the control. With a local vorticity thickness of approximately 30 mm (deduced from Fig 3a), a convection velocity of 4.4 m/s can be estimated. This is almost equal to the value deduced from the characteristics of coherent structures due to the synthetic jets. The convective behavior of the synthetic jet is revealed such that the phase in mode 2 (Fig. 11b) has been shifted by π approximately with respect to mode 1 (Fig. 11a) in the downstream direction. This is a direct consequence of traveling waves in the flow.

The mixing layer starts to reveal itself in the third mode along the axis $y \sim 0$ mm as shown in Fig. 12a. Character of the synthetic jet is also present in the region where $y < 0$ mm. Spatial modes three and four can be interpreted to be the coherent structures due to the interaction between the original mixing layer and the synthetic jet. It is important to note that the high level of coherence of structures due to the synthetic jet, presented in Fig. 11, allows itself to be decoupled from the rest of the modes.

3.3. Deflecting mixing layer in the far field of the jet

To exemplify the effectiveness of the synthetic jet, a PIV experiment is performed on a larger observation window size. Due to experimental constraints, the flow configuration is slightly different. A velocity ratio $r = 0.6$ is maintained with $U_1 = 2.35$ m/s. The jet is deployed at a frequency of 60 Hz with a peak velocity of 27 m/s and the splitter plate is 70 mm above the flat plate in which the loud speakers are installed. As shown in Fig. 13, the mixing layer has been deviated such that it almost comes into contact with the wall surface. The streamwise and vertical velocity profiles for both uncontrolled and controlled cases are shown in Fig. 14a and b, respectively. The vorticity thickness, in the natural case, follows approximately the Abramovich–Sabin rule for plane mixing layers shown in Fig. 14c. The uncontrolled stream-

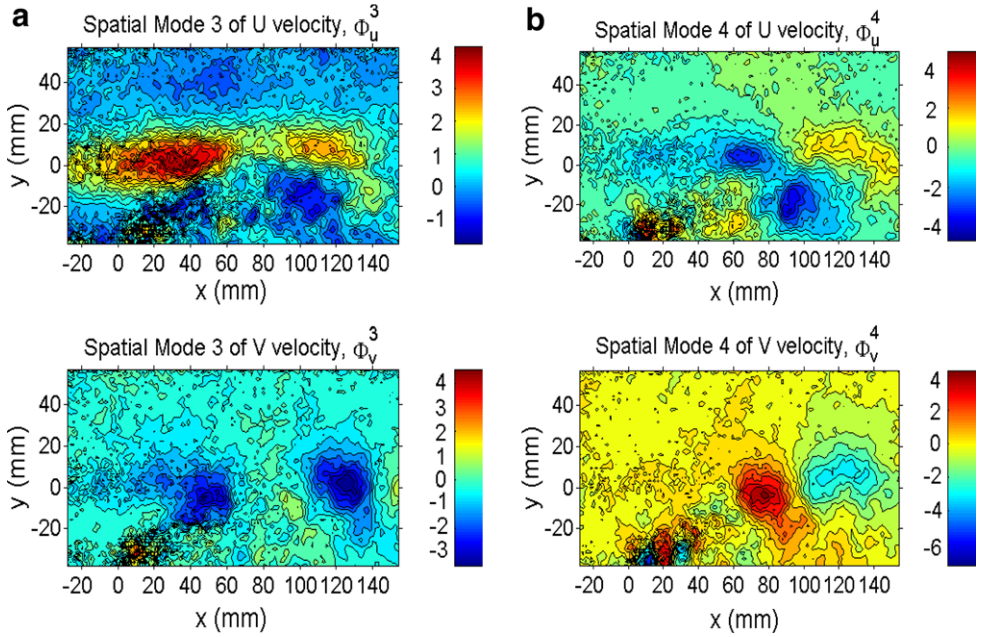

Fig. 12. Spatial modes for U and V velocities for the controlled flow: (a) third; and (b) fourth mode.

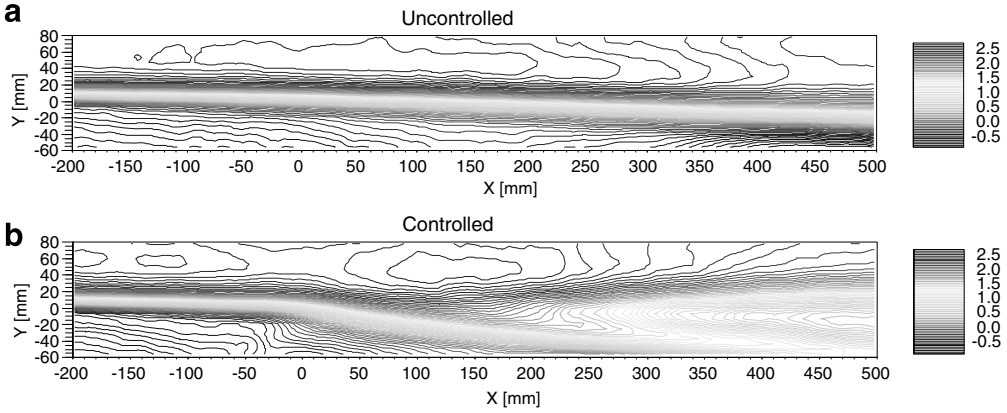

Fig. 13. U velocity contour for: (a) uncontrolled; and (b) controlled case, with synthetic jet deployed at 60 Hz.

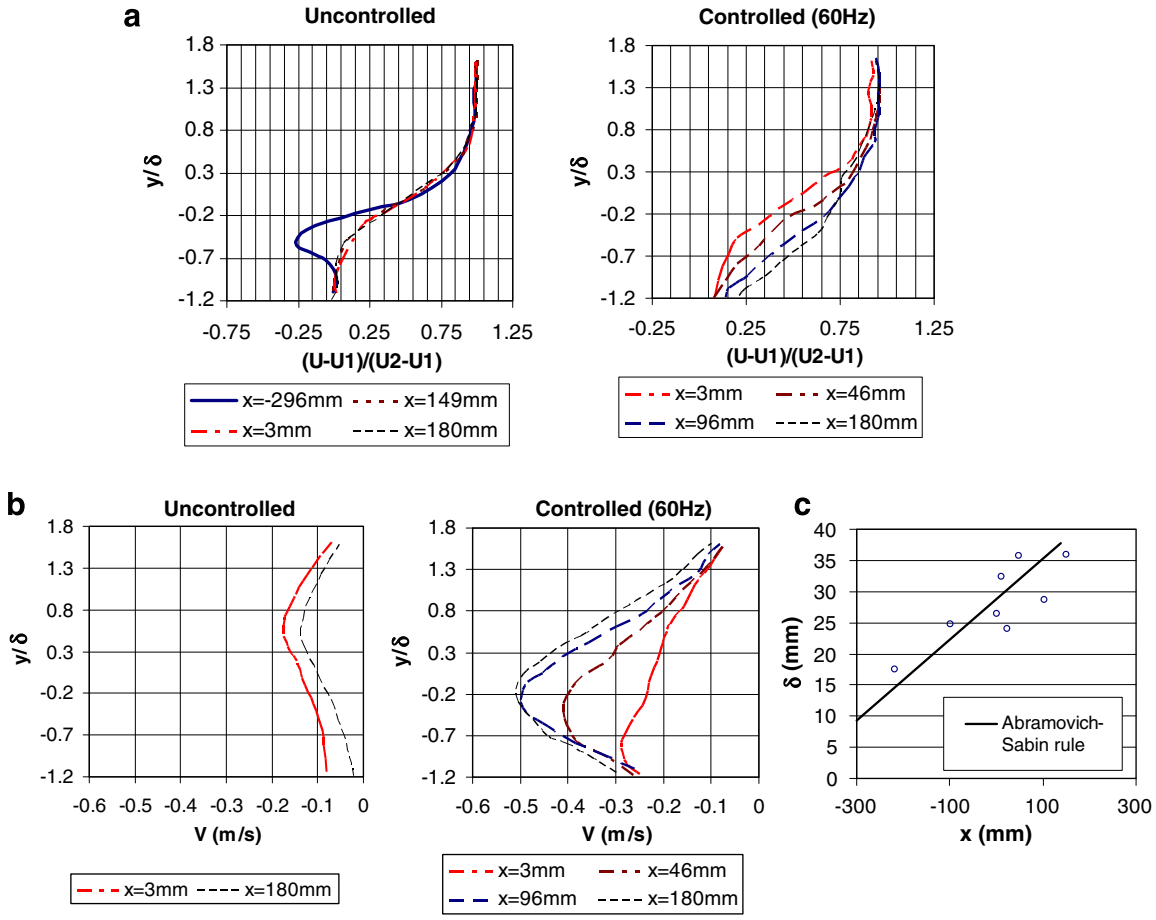

Fig. 14. Velocity profile for: (a) U component; (b) V component; and (c) vorticity thickness distribution of the uncontrolled flow.

wise velocity profiles in Fig. 14a reveals a wake effect near the trailing edge of the splitter plate ($x = -296$ mm). This effect rapidly disappears and the mixing layer behaves in a self-similar way at the synthetic jet location of $x = 0$ mm. For the controlled case, the increase in streamwise velocity and a larger mean vertical velocity towards the wall for $y/\delta < 0$ indicate that the shear layer is displaced towards the wall. With reference to Fig. 15b, a large increase of turbulent energy is observed downstream of the interacting region defined as the regions for which $x > 180$ mm (note that the iso-levels do not have the same contour scales in Fig. 15). From the point of view of turbulent activity, the flow has been split into two distinct regions: the upper region corresponding to the turbulent activity generated by the synthetic jet; and the lower region corresponding to the deviated mixing layer which has a lower turbulent energy when it approaches the wall. The high turbulent energy is attributed to the high velocity gradients generated as a result of the interaction of the synthetic jet and the deviated mixing layer. The overall turbulent energy in the interacting region increases by at least one order of magnitude.

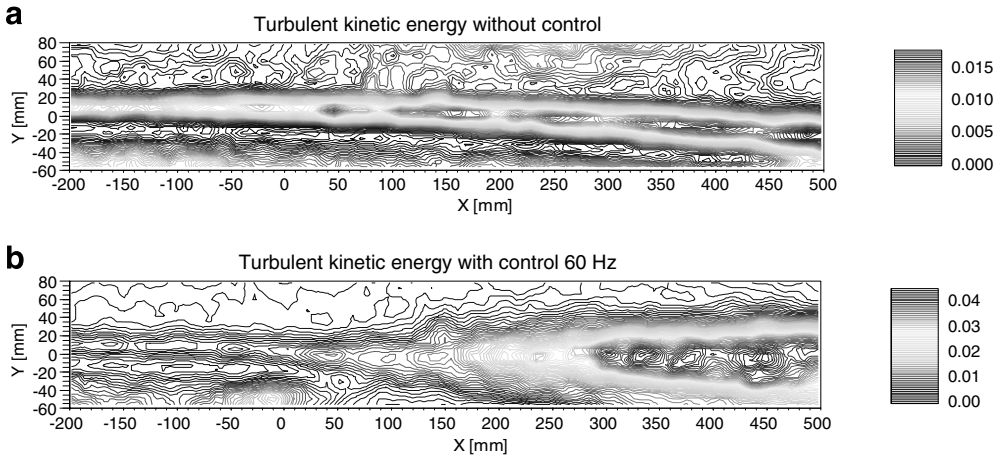

Fig. 15. Turbulent energy ($\langle u'^2 \rangle + \langle v'^2 \rangle$) for: (a) uncontrolled; and (b) controlled flow, with jets deployed at 60 Hz.

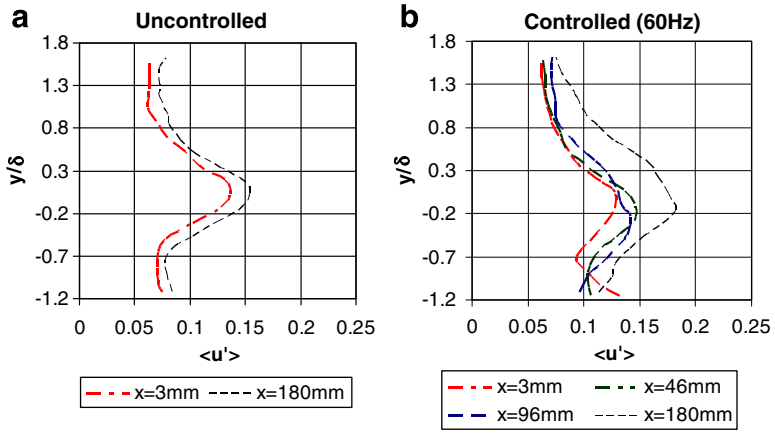

Fig. 16. Streamwise velocity fluctuations: (a) uncontrolled; and (b) controlled flow.

By comparing the profiles of the streamwise velocity fluctuating component at $x = 3$ mm, 46 mm and 96 mm, for the uncontrolled (Fig. 16a) and controlled cases (Fig. 16b), it can be seen that there is an overall downward shift of the main maximum towards the wall when the jet is deployed. This is due to the deviation of the mixing layer towards the wall. At $x = 3$ mm, a second maximum occurs towards the wall surface which is contributed by the high velocity gradient in the near field of the synthetic jet. The same has been observed in Fig. 7a in Section 3.1. At $x = 180$ mm, an upward shift of the maximum is observed and is due to the turbulent activity generated by the synthetic jets.

With reference to Fig. 17a and b, the absolute value of the turbulent shear stress profile at $x = 3$ mm and $y/\delta \sim 0$ is decreased when the jet is deployed and there is a slight downward shift of the minimum. There is an overall increase in the value of the shear stress towards the wall. This observation is consistent with the $\langle u'v' \rangle$ contour distribution in the vicinity of the synthetic jet in Fig. 8a. At $x = 180$ mm, the absolute value of the shear stress increases and no observable shift in the minimum.

3.4. Influence of the velocity ratio $U_{jet\text{-}peak}/U_m$

In this section, three test cases are presented concerning the effects of increasing the velocity of the wind tunnel while maintaining the same velocity ratio of the mixing layer (r) and synthetic jet velocity. The test cases are tabulated in Table 2. The test setup is the same as that in Section 3.1. In this section, it is preferred to analyse the total velocity field because it reveals the core of the vortex ring more clearly. We use the model of Hasselbrink and Mungal (2001) to estimate the trajectory of the synthetic jet: $y/r_d = (2/C_{ej} \cdot x/r_d)^{1/2}$ (where $r_d = U_{jet}/U_2 \cdot d_{jet}$, d_{jet} is the diameter of the orifice and $C_{ej} = 0.32$). Difficulties associated to this model in our present case are as follows: (1) U_{jet} in the present case is unsteady thus it is not easy to define a global length scale, "$U_{jet}/U_2 d_{jet}$"; (2) the interaction between the mixing layer and the synthetic jet (also interaction between synthetic jet) is not modelled in the equation; and (3) it is not sure that the peak velocity at the orifice is the same in wind on and off condition. According to Li et al. (2006), in the presence of a cross flow, the maximum velocity of a continuous jet would decrease by 90% for S/d of more than 15, where "S" is the length of the trajectory and "d" is the diameter of the orifice. Thus, for a peak velocity of 40 m/s, we estimate a U_{jet} of 4 m/s (40×0.1 m/s). Drawing the same analogy from Li et al. (2006), it is not surprising that the total velocity contours in Fig. 18 do not register a velocity of more than 5 m/s. The plot of S/d versus x is plotted in Fig. 19, it can be observed that $S/d = 15$ occurs at $x \sim 30$ mm. The order of magnitude of the velocity, in the vicinity of $x \sim 30$ mm, is consistent with (Fig. 18). At this distance, as

Table 2
Test conditions for parametric study

U_1 (m/s)	r	ΔU	$U_{jet\text{-}peak}/U_m$
4.8	0.62	1.69	10
3.86	0.63	1.43	12.7
2.42	0.63	0.93	20.5

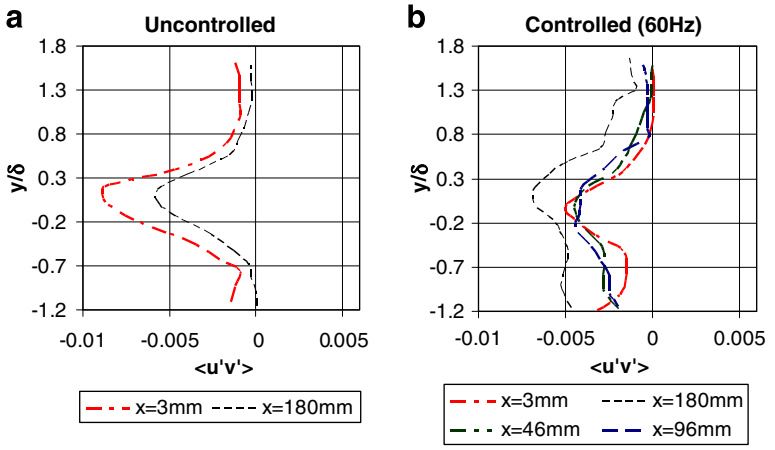

Fig. 17. Turbulent shear stress profiles: (a) uncontrolled; and (b) controlled flow.

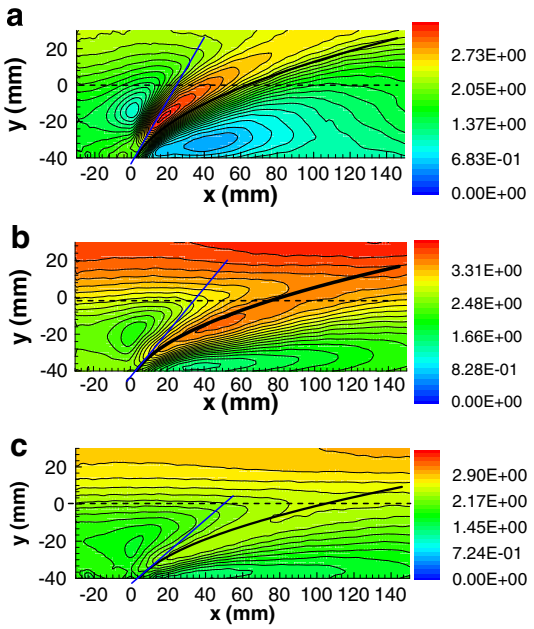

Fig. 18. Total velocity field $(U^2 + V^2)^{0.5}$ with $U_{\text{jet-peak}}/U_{\text{m}}$ equal: (a) 20.5; (b) 12.7; and (c) 10.

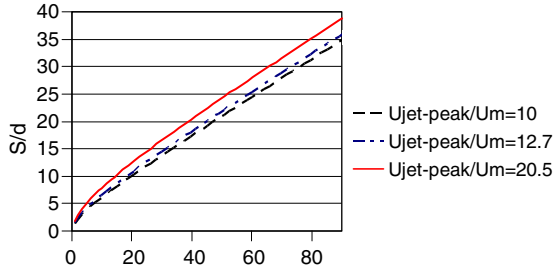

Fig. 19. The variation of the length of the trajectory (S) non-dimensionalised by (d, diameter of the orifice) for different $U_{\text{jet-peak}}/U_{\text{m}}$.

documented in Bourgois (2007), the suction phase of the synthetic jet according to the hotwire is virtually absent (i.e. approaching a steady jet characteristic) and thus might partially validate the use of the trajectory equation as an approximate model.

The trajectories superimposed onto the total velocity field for various $U_{\text{jet-peak}}/U_{\text{m}}$ are plotted on (Fig. 18). It seems that the control jet tends to negotiate the path of maximum total velocity. With reference to Fig. 18a, the trajectory of the jet penetrates the mixing layer completely when $U_{\text{jet-peak}}/U_{\text{m}} = 20.5$. The contour distribution of the original mixing layer is not present and the velocity has been reduced in the region of $y < 0$ mm and $x > 0$ mm. In this case the jet behaves as if it is a "barrier" to the upcoming flow.

It is possible that the synthetic jet will cause massive separation at the actuation location if $U_{\text{jet-peak}}/U_{\text{m}}$ is increased beyond 20.5. As $U_{\text{jet-peak}}/U_{\text{m}}$ is decreased by increasing the upstream velocity, it can be seen that the trajectory of the synthetic jet (Fig. 18b and c) is skewed towards wall such that the entrainment process increases the velocity between the wall and the mixing layer ($y < 0$ mm and $x > 0$ mm). This change in flow structure is perceived as a deflection of the original mixing layer. This observation offers a guide to optimise the entrainment process for a particular flow configuration. By inspecting the magnitude of the velocity along the jet trajectories, we deduce that the decay of the velocity from a peak value of 40 m/s at the orifice exit is more drastic when the gradient of the trajectory near to the vicinity of the jets is larger as in Fig. 18a. Work of Li et al. (2006) has the same observation for a continuous jet deployed in a crossflow.

4. Conclusion

A mixing layer close to a solid wall has been modified by synthetic jets in order to simulate a control scenario acting within a region of separation. The control was performed with synthetic jets perturbing the mixing layer in its developed region. It has been shown that the deployment of the synthetic jets results in a deviation of the mixing layer. This is due to the enhance mixing of the synthetic jet in the low velocity side of the mixing layer. Observation from a larger PIV window indicated that the deflected mixing layer approaches very close to the lower wall and that the resulting turbulent field is split into two parts downstream of the "reattachment" position. The upper and lower portions correspond to the synthetic jet and the deviated mixing layer, respectively. The upper portion is viewed as loss of useful energy and could be the cost for such a specific control method. It is also observed that the displaced mixing layer has lower turbulent energy toward the wall surface.

The fluctuating streamwise velocity and shear stress, obtained from the PIV results in the near field of the synthetic jet, is consistent with the results obtained from a larger PIV observation window. The main difference was that the interaction region as defined in Section 3.3. was not within the field of view. The POD analysis in the near field of the synthetic jet showed a strong reorganization of the flow downstream of the interaction. The structure of the synthetic jet can be decoupled from the main flow via POD. Moreover a vortex ring structure and its convective behavior are revealed. Parametric studies by varying the tunnel velocity indicated that efficient mixing is dependent on the ratio of the peak synthetic jet velocity and low velocity side of the mixing layer. An efficient ratio would depend on the model configuration, and the distance between the mixing layer and actuator. This analysis could lead to further improvements in terms of the deflection of the mixing layer by using an actuation frequency that perturbs the base instability within the mixing layer. In the current state of technology, it is difficult to attain a peak synthetic jet velocity in excess of 100 m/s in order to attain a realistic velocity ratio that is important for practical application. Nevertheless, the information in this paper would provide interpretation of the flow control mechanism by synthetic jets.

Acknowledgements

The authors gratefully thank M. Jean-Marc Breux for his help in experiments and data processing; and M. Vassili Kitsios for proof reading the paper.

References

Amitay, M., Glezer, A., 2002. Controlled transients of flow reattachment over stalled airfoil. International Journal of Heat and Fluid Flow 25, 351–363.
Bourgois, S., 2007. Etude expérimentale du décollement sur profils d'aile: analyse et contrôle. Thèse Doctorat, Université de Poitiers.
Darabi, A., Wygnanski, I., 2004. Active management of naturally separated flow over a solid surface Part 1. The attachment process. Journal of Fluid Mechanics 510, 105–129.
Darabi, A., Wygnanski, I., 2004. Active management of naturally separated flow over a solid surface. Part 2. The separation process. Journal of Fluid Mechanics 510, 31–144.
Delville, J., Cordier, L., Bonnet, J.P., Glauser, M., 1999. Examination of large scale structures in a turbulent plane mixing layer. Journal of Fluid Mechanics 391, 91–122.
Hasselbrink, E., Mungal, M., 2001. Transverse jets and flames. Part 1: Scaling laws for strong transverse jets. Journal of Fluid Mechanics 443, 1–25.
Ho, C.M., Huerre, P., 1984. Perturbed free shear layers. Annual Review of Fluid Mechanics 16, 365–424.

Hong, G., Lee, C., Ha, Q., Mack, A.N.F., Mallinson, S.G., 2002. Effectiveness of synthetic jets enhanced by instability of Tollmien–Schlichting waves. AIAA paper 2002-2832, 1st AIAA Flow Control Conference, St Louis, MO, USA, June 2002.

Li, Z., Murugappan, S., Gutmark, E., Vallet, L., 2006. Numerical simulation and experiments of jets in cross flow. In: 44th AIAA Aerospace Sciences Meeting and Exhibit 9–12 January 2006, Reno, Nevada, AIAA 2006-307.

Lumley, J.L., 1967. The structure of inhomogeneous turbulent flows. Atm. Turbulence and Radio Wave Prop., Moscow.

Viswanath, P., Ramesh, G., Madhavan, K., 2000. Separation control by tangential blowing inside the bubble. Experiments in Fluids 29, 96–102.

Yehoshua, T., Seifert, A., 2006. Active boundary layer tripping using oscillatory vorticity generator. Aerospace Science and Technology 10, 175–180.